Effect of Axial Loading on Quench Performance in Nb_3Sn Magnets

P. Ferracin, G. Ambrosio, B. Bordini, S. Caspi, D. R. Dietderich, H. Felice, A. R. Hafalia, C. R. Hannaford, J. Lizarazo, A. F. Lietzke, A. D. McInturff, G. L. Sabbi, J. D. DiMarco, M. Tartaglia, and P. Vedrine

***Abstract*— A series of tests has been performed at Lawrence Berkeley National Laboratory (LBNL) and Fermi National Accelerator Laboratory (FNAL) with the goal of assessing the influence of coil axial pre-load on Nb_3Sn magnet training. The tests involved two subscale Nb_3Sn magnets: SQ02, a quadrupole magnet fabricated as part of the US LHC Accelerator Research Program (LARP), and SD01, a dipole magnet developed in collaboration between CEA/Saclay and LBNL. Both magnets used similar Nb_3Sn flat racetrack coils from LBNL Subscale Magnet Program, and implemented an axial support system composed of stainless steel end-plates and aluminum rods. The system was designed to withstand full longitudinal electro-magnetic forces and provide controllable preloads. Quench performances, training, and quench locations have been recorded in various axial loading conditions. Test results are reported.**

Index Terms— LARP, superconducting magnets, Nb_3Sn.

I. INTRODUCTION

WHEN a superconducting magnet for particle accelerator is energized, the axial electro-magnetic (e.m.) forces tend to elongate the coil along the longitudinal direction. The induced coil frictional motion, as well as the epoxy cracking in an impregnated coil, may cause premature quenches and limit the magnet performance [1]. For this reason, the US LHC Accelerator Research Program (LARP [2]), is investigating, within the Technology Quadrupole Program (TQ [3]-[4]), the affects of different axial support systems in preventing motion-induced quenches in Nb_3Sn superconducting coils. As part of the study, the LARP collaboration has also launched a series of tests with subscale quadrupole magnet SQ02 [5] assembled with different axial loading conditions. Concurrently, the Superconducting Magnet Group at LBNL has investigated the importance of the axial support on the subscale dipole SD01, developed in collaboration with CEA-Saclay [6]. The two magnets have been tested with and without axial end loads. In this paper, after a description of magnet designs, the test results are presented.

Manuscript received August 28, 2007. This work was supported by the Director, Office of Energy Research, Office of High Energy and Nuclear Physics, High Energy Physics Division, U. S. Department of Energy, under Contract No. DE-AC02-05CH11231.

P. Ferracin, S. Caspi , D. R. Dietderich, H. Felice, A. R. Hafalia, C.R. Hannaford, J. Lizarazo, A. F. Lietzke, A.D. McInturff, and G. L. Sabbi are with Lawrence Berkeley National Lab, Berkeley, CA 94720, USA (phone: 510-486-4630; fax: 510-486-5310; e-mail: pferracin@lbl.gov).

B. Bordini was with Fermi National Accelerator Laboratory. He is now with European Organization for Nuclear Research, Geneva, Switzerland.

G. Ambrosio, J. D. DiMarco, and M. Tartaglia are with Fermilab National Accelerator Laboratory, Batavia, IL 60510-0500, USA.

P. Vedrine is with CEA/Saclay, DAPNIA/SACM/LEAS, 91191 Gif-Sur-Yvette Cedex, France.

II. MAGNET DESIGNS AND PARAMETERS

The cross-sections of SQ02 and SD01 are shown in Fig. 1 (see [7] and [6], respectively, for a detailed description of the magnet designs). The magnets implement Nb_3Sn racetrack coils (SC16-SC17-SC18-SC19 in SQ02 and SC01- SC02 in SD01) originally designed for the LBNL Subscale Magnet Program [8]. In SQ02, four coils with aluminum-bronze winding poles are mounted around an aluminum bore in a quadrupole configuration. In SD01, two coils, wound around iron poles, are combined to generate a dipole field.

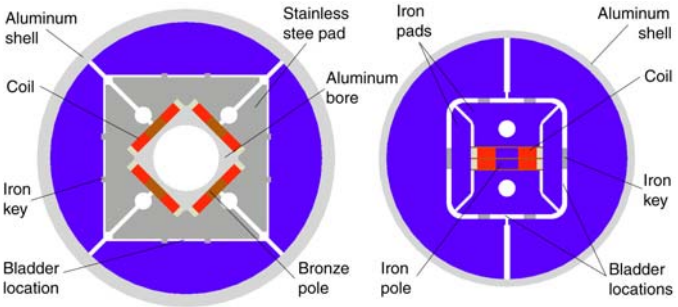

Fig. 1. SQ02 (left) and SD01 (right) cross-sections.

The coils are surrounded by 4 pads bolted together, and by a four-piece (SQ02) or two-piece (SD01) iron yoke contained in an aluminum shell. The structure is pre-loaded with water-pressurized bladders inserted in the slots between pads and yoke. During the cool-down, due to the different thermal contraction of aluminum and iron, the shell shrinkage increases the pre-load on the coil-pack. The axial support systems (see Fig. 2) are composed of aluminum rods connected to two stainless steel endplates.

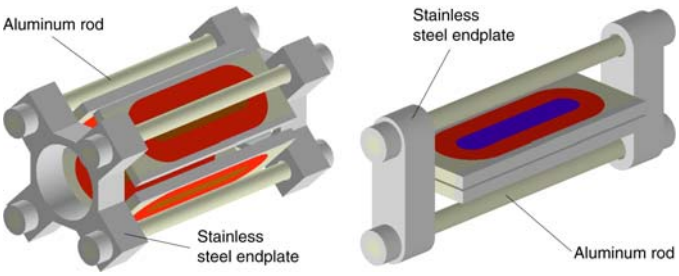

Fig. 2. SQ02 (left) and SD01 (right) axial support system.

TABLE I CABLE AND MAGNET PARAMETERS

	Unit	SQ02	SD01
N of double-layer coils		4	2
Number of turns per layer		21	20
Strand diameter	mm	0.700	0.700
Number of strands		20	20
Cable width (bare)	mm	7.793	7.938
Cable thickness (bare)	mm	1.276	1.280
Insulation thickness	mm	0.092	0.100
Cu/Sc ratio		0.89	0.81
J_c (12 T, 4.2 K)	A/mm^2	1870	2334
RRR		300	38
B_{peak} (4.3 K)	T	11.1	12.5
I_{ss} (4.3 K)	kA	9.9	8.8
I_{ss} (4.3 K) per strand	A	494	438
F_z per coil @ I_{ss}	kN	83	85

The rods are pre-tensioned at room temperature with a hydraulic piston in a specially designed fixture, and, as with the pre-loaded aluminum shell, during cool-down, their contraction imparts a significant increase in the axial load.

Table I shows the main parameters for the two magnets, estimated according to measurements of the strand witness samples accompanying the coils during their respective heat treatments. SQ02 has a short sample current at 4.3 K of 9.9 kA with a conductor peak field of 11.1 T. SD01 reaches a maximum field of 12.5 T at a current of 8.8 kA. It can also be noted that the two magnets generate similar axial e.m. forces (about 84 kN per coil).

III. LOADING PROCEDURES AND TEST RESULTS

A. SQ02

SQ02 was assembled and pre-loaded at LBNL, and it underwent three tests: SQ02 (two thermal cycles) at the LBNL magnet test facility (at 4.3 K), and SQ02b and SQ02c at the FNAL magnet test facility (at 4.5 K and 1.8 K). In Fig. 3 and Fig. 4, the shell and rod stress histories and the quench performance are shown, respectively. The first two thermal cycles of SQ02 (see [5] for the complete test report) were performed with a tensile stress of 95 MPa in the shell and 125 MPa in the rods after cool-down to 4.3 K . During the first thermal cycle, the magnet trained from 5.9 kA (60% of I_{ss}) up to a maximum current of 9.4 kA (96% of I_{ss}). In the second thermal cycle, the first quench occurred at the same current level as the maximum current of the first thermal cycle (full training "memory") and a plateau current of about 9.6 kA (97% of I_{ss}) was achieved. All the plateau quenches occurred in the high field region (pole turn, return end) of coil SC18. The second test (SQ02b) was performed with a shell stress similar as SQ02, but with a tension in the rods of 190 MPa after cool-down. The increase in applied axial force did not produce a significant change in the magnet performance with respect to the second thermal cycle of SQ02. In fact, SQ02b reached a maximum current corresponding to about 97% of I_{ss} both at 4.5 K and 1.8 K, with the plateau quenches still located in the high field region of coil SC18. After warm-up, the axial pre-load was released at LBNL, and the magnet was sent back and tested again as SQ02c at FNAL. The first quench at 4.5 K occurred at a slightly lower current than in SQ02b, but after few quenches the magnet reached the previous maximum current (about 96% of I_{ss}), still in SC18. At this point, the conclusion was that, in a magnet already trained (not virgin), the absence of axial support does not produce a significant variation in the magnet performance.

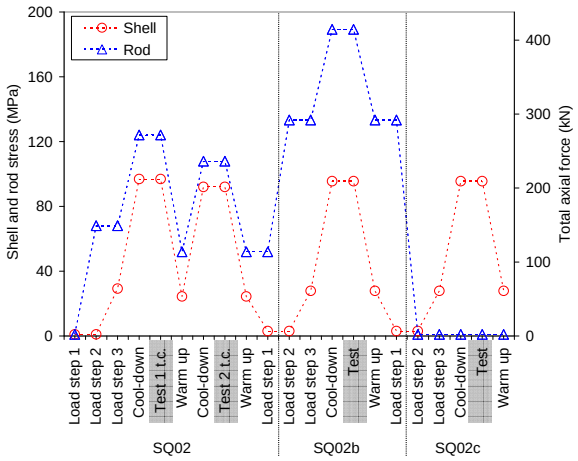

Fig. 3. Measured (from SQ02 "Load step 1" to SQ02b "Test") and expected (from SQ02b "Warm up" to SQ02c "Warm up") stress in shell and rod (left axis) and total applied axial force (right axis) during loadings and tests of SQ02, SQ02b, and SQ02c.

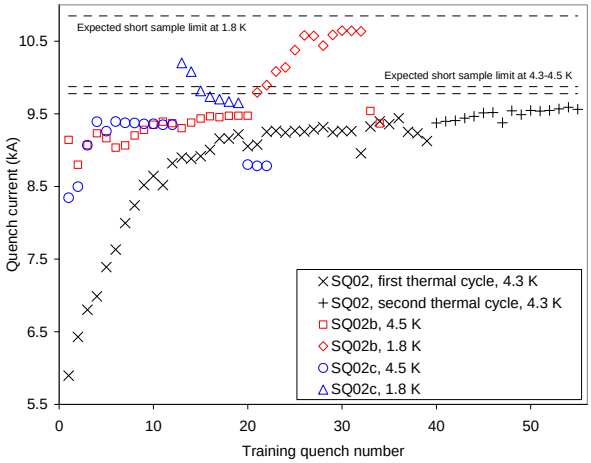

Fig. 4. Training performance of SQ02 (two thermal cycles at 4.3 K), SQ02b (at 4.5 K and 1.8 K), and SQ02c (at 4.5 K and 1.8 K). The dashed lines represent the expected current limits based on strand measurements.

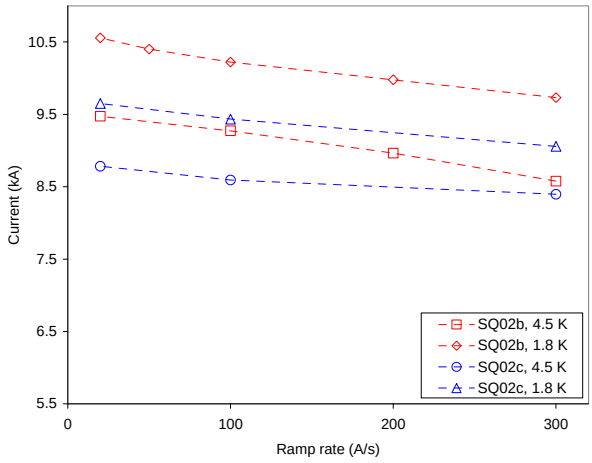

Fig 5. SQ02b and SQ02c ramp-rate dependence of quench current at 4.5 K and 1.8 K.

Nevertheless, after cool-down to 1.8 K, SQ02c experienced

a first quench at 10.2 kA, followed by a series of quenches progressively at lower current and all located in a new coil (SC17). In other words, when the axially unsupported magnet was energized to a level of current (and forces) approaching the 1.8 K limit, the coils showed a degradation of 1000 A with respect the 1.8 K maximum current achieved during the SQ02b test. Moreover, when the magnet was warmed-up again to 4.5 K and energized, the quench current appeared degraded of about 600 A (with quenches still in coil SC17). Also the ramp-rate dependence studies, performed at the end of the SQ02b and SQ02c both at 4.5 K and 1.8 K (see Fig. 5) confirmed the degradation observed during magnet trainings.

B. SD01

SD01 was assembled, loaded, and tested at LBNL. A total of four tests were performed: SD01, SD01b, SD01c, and SD01d. Fig. 6 and Fig. 7 show respectively the shell and rod stress histories over the four tests, and the quench performance recorded in the first two. The first test (see [6] for a complete test report) was carried out with a tension of 135 MPa in the shell and 190 MPa in the axial rods after cool-down to 4.3 K (see Fig. 6).

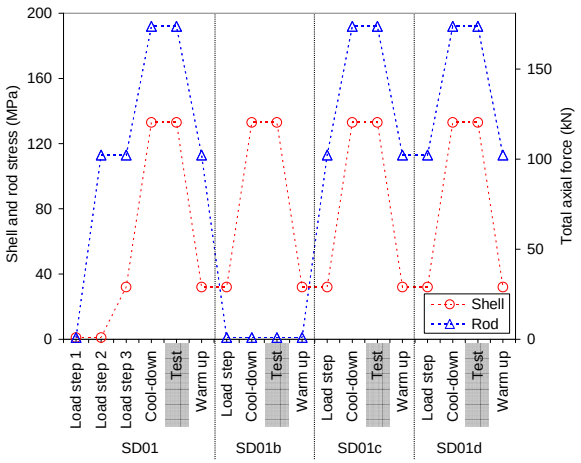

Fig. 6. Measured (from SD01 "Load step 1" to SD01 "Test") and expected (from SD01 "Warm up" to SD01d "Warm up") stress in shell and rod (left axis) and total applied axial force (right axis) during loadings and tests of SD01, SD01b, SD01c, and SD01d.

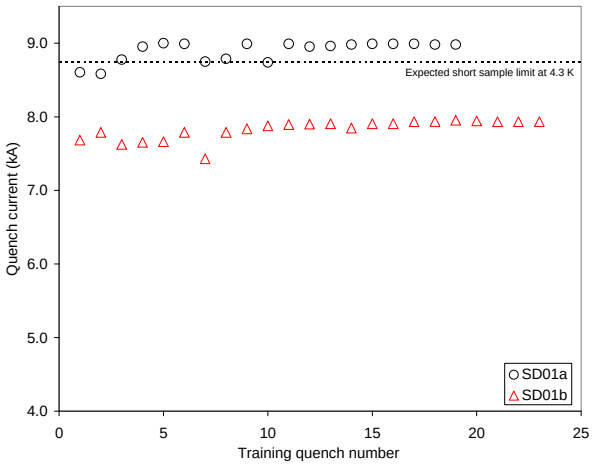

Fig. 7. Training performance of SD01 and SD01b at 4.3 K. The dashed line represents the expected current limits based on strand measurements.

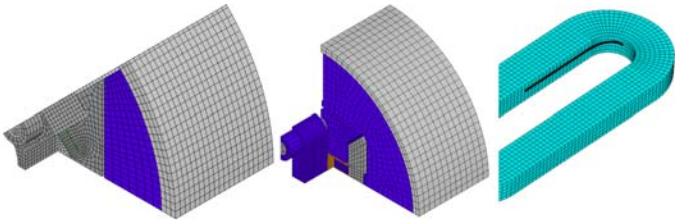

Fig. 8. Finite element model of SQ02 (left), SD01 (center) and details of the coil mesh (left). The black line on the inner surface of the coil indicates the path along which the coil strain has been computed.

The magnet trained from 8.6 kA up to a current plateau of 9.0 kA, about 2% higher than the predicted short sample current. All the quenches were located in coil SC02 (a coil fabricated early in the Subscale Magnet Program) but due to a lack of voltage taps, it was not possible to determine the quench locations. After warm-up, the axial support system was removed, and the magnet retested as SD01b. The first quench of SD01b occurred at 7.7 kA, and a stable plateau was reached at about 7.9 kA with quenches distributed in both coils. As previously observed in SQ02c, the removal of the axial support induced a significant decrease in the maximum current. At this point, in order to check if the degradation was reversible, a re-loading of the axial rods performed, with the magnet at room temperature and still attached to the header. The magnet was cooled down and re-tested, but the coil quenched at an anomalous low current. After the magnet was warmed up and inspected, it was noticed that one of the G10 shims transferring axial loads between end plate and the coils had shifted during cool-down, and the entire axial force from the rods was applied only to one coil. A fourth test, performed with the axial support providing load uniformly to both coils, did not show any improved performance.

IV. Analysis

In order to investigate the possible causes of the SQ02 and SD01 performance degradation, the strain status of the coils was investigated using 3D finite element mechanical models (see Fig. 8). The analyses focused on the effect of the axial e.m. forces on the strain in the pole turn.

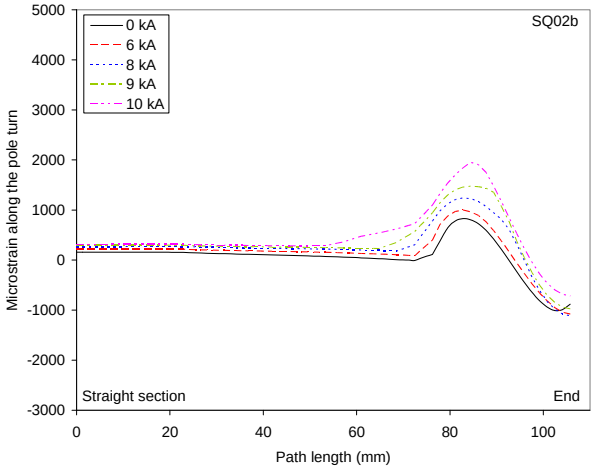

Fig. 9. Computed strain during excitation along the cable on a path moving from the center of the straight section to the end, in the SQ02b conditions (full axial support).

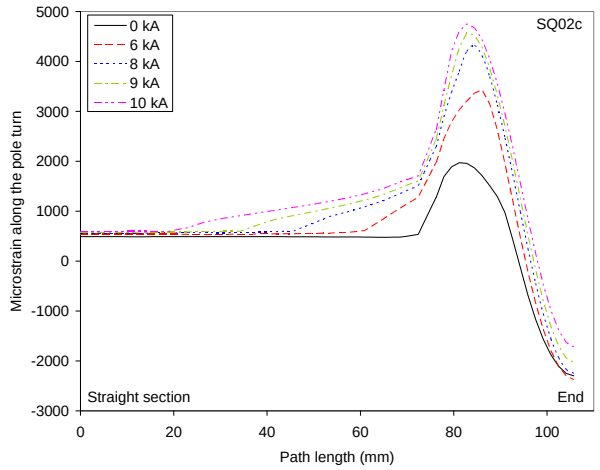

Fig. 10. Computed strain during excitation along the cable on a path moving from the center of the straight section to the end, in the SQ02c conditions (no axial support).

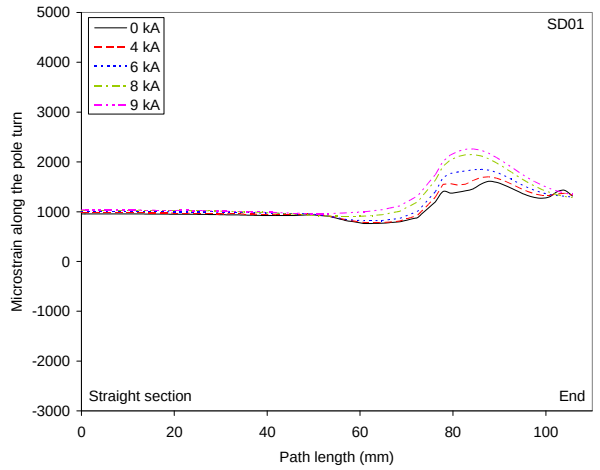

Fig. 11. Computed strain during excitation along the cable on a path moving from the center of the straight section to the end, in the SD01 conditions (full axial support).

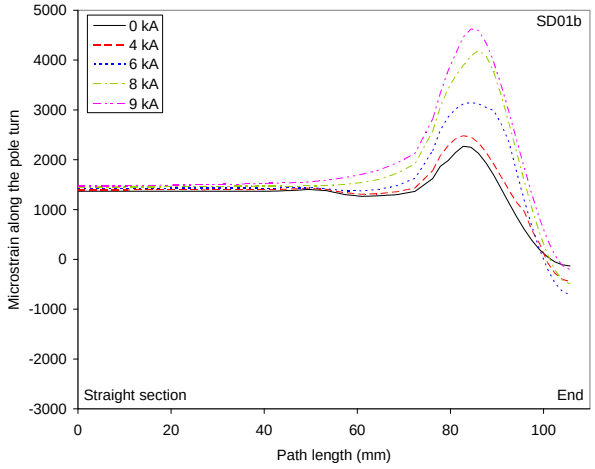

Fig. 12. Computed strain during excitation along the cable on a path moving from the center of the straight section to the end, in the SD01b conditions (no axial support).

A path moving from the center of the straight section to the center of the end (see black line in Fig. 8, left) was considered, and the pole turn strain in the direction along the conductor was evaluated. As depicted in Fig. 9, when the situation with full axial load of SQ is simulated (SQ02b), the cable strain is expected to vary from + 2000 microstrain at the end of the straight section (about 76.2 mm) to – 1000 microstrain in the tip of the end. When the axial support is removed (SQ02c case in Fig. 10), because of the bending induced by the e.m. forces on the unsupported end region, the gradient of strain significantly increases: from a tension of almost 5000 microstrain at the beginning of the end, the cable experiences a compression of more than 2000 microstrain at the center of the end. A similar effect is noticed for SD01 (see Fig. 11) and SD01b (Fig. 12). In this case, the cable is partially in tension in the straight section, because of the low thermal contraction of the iron pole, and reaches almost 5000 microstrain of tension in the end when the axial rods are not included.

V. Discussions and Conclusions

Two Nb_3Sn subscale magnets, SQ02 and SD01, were tested in various axial loading conditions to investigate the effect of axial support on quench performance. Even though both magnets reached their expected short sample current limits when fully supported, they showed a clear degradation in training performance (in the order of 5 to 10% in quench current) when no axial load was applied. On the one hand, in the SQ02 case, the degradation was progressive over consecutive quenches, i.e., the quench current gradually decreased from a value of 10.2 kA to 9.7 kA in seven quenches. On the other hand, in the SD01 case, the degradation was more abrupt, with an offset in quench current of about 1 kA.

A 3D finite element analysis pointed out, as a possible cause of the performance degradation when the axial support is removed, a high tensile strain (about 5000 microstrain) at the end of the straight section, followed by about 2000 microstrain of compression in the tip of the end. At this stage of the study, the question regarding the possibility of recovering from the degradation by re-applying the axial load remains unanswered, since the attempt in SD01 was aborted because of an assembly fault.

References

[1] A. F. Lietzke, *et al.*, "Test results for HD1, a Nb3Sn dipole magnet", *IEEE Trans. Appl. Supercond.*, vol. 14, no. 2, June 2004, pp. 345-348.

[2] S.A. Gourlay, *et al.*, "Magnet R&D for the US LHC Accelerator Research Program", *IEEE Trans. Appl. Supercond.*, vol. 16, no. 2, June 2006, pp. 324-327.

[3] S. Caspi, *et al.*, "Design and analysis of TQS01, a 90 mm Nb_3Sn model quadrupole for the LHC luminosity upgrade based on a key and bladder assembly", *IEEE Trans. Appl. Supercond.*, vol. 16, no. 2, June 2006, pp. 358-361.

[4] R.C. Bossert, *et al.*, "Development of TQC01, a 90 mm Nb_3Sn model quadrupole for the LHC upgrade based on SS collars", *IEEE Trans. Appl. Supercond.*, vol. 16, no. 2, June 2006, pp. 370-373.

[5] P. Ferracin, *et al.*, "Assembly and Tests of SQ02, a Nb_3Sn Racetrack Quadrupole Magnet for LARP", *IEEE Trans. Appl. Supercond.*, vol. 17, no. 2, June 2007, pp. 1019-1022.

[6] H. Felice, *et al.*, "Design and Test of a Nb_3Sn Subscale Dipole Magnet for Training Studies", *IEEE Trans. Appl. Supercond.*, vol. 17, no. 2, June 2007, pp. 1144-1148.

[7] P. Ferracin, *et al.*, "Development of a large aperture Nb_3Sn racetrack quadrupole magnet", *IEEE Trans. Appl. Supercond.*, vol. 15, no. 2, pp. 1132-1135, June 2005.

[8] A. R. Hafalia, *et al.*, "An approach for faster high field magnet technology development", *IEEE Trans. Appl. Supercond.*, vol. 13, no. 2, June 2003, pp. 1258-1261.